Multibody Syst Dyn (2011) 25: 167–183
DOI 10.1007/s11044-010-9230-y

Dealing with multiple contacts in a human-in-the-loop application

Daniel Dopico · Alberto Luaces · Manuel Gonzalez · Javier Cuadrado

Received: 23 November 2009 / Accepted: 23 September 2010 / Published online: 27 October 2010

Abstract This paper deals with continuous contact force models applied to the human-in-the-loop simulation of multibody systems, while the results are valid in general to all the real-time applications with contacts. The contact model proposed in this work is suited to collisions between massive solids for which the assumption of quasi-static contact holds, and it can be supposed that the deformation is limited to a small region of the colliding bodies while the remainder of them are assumed to be rigid. The model consists of two components: normal compliance with nonlinear viscoelastic model based on the Hertz law, and tangential friction force based on Coulomb's law including sticktion and a viscous friction component. Furthermore, the model takes into account the geometry and the material of the colliding bodies. The tangential model is a novel contribution while the normal model is completely taken from previous works. For this work, the formulation of the equations of motion is an augmented Lagrangian with projections of velocities and accelerations onto their constraints manifolds and implicit integrator. The whole solution proposed is tested in three applications: the first one is the simulation of a spring–mass system with Coulomb's friction, which is an academic problem with known analytical solution; the second one is the Bowden and Leben stick–slip experiment; the third one is a simulator of a hydraulic excavator Liebherr A924, which is a realistic application that gives an idea of the capabilities of the method proposed.

Keywords Multibody dynamics · Real time · Contact

D. Dopico (✉) · A. Luaces · M. Gonzalez · J. Cuadrado
Escuela Politecnica Superior, Universidad de A Coruña, Mendizabal s/n, 15403 Ferrol, Spain
e-mail: ddopico@udc.es

A. Luaces
e-mail: aluaces@udc.es

M. Gonzalez
e-mail: lolo@cdf.udc.es

J. Cuadrado
e-mail: javicuad@cdf.udc.es
url: http://lim.ii.udc.es/index.en.html

1 Introduction

The treatment of contact forces is a key issue in many applications involving multibody systems with eventual impacts or permanent contacts between bodies. If the application to address includes also human-in-the-loop, this treatment has to be even more careful because the real-time requirements impose firm constraints on the integration time-step and, additionally, on the number of iterations if implicit integration is used. In addition to the efficiency considerations, the simulation has to be stable and robust enough along all the range of possible operations of the system, as well as reproduce the behavior of the real system with an acceptable precision.

To solve the impact problem in multibody systems composed of rigid bodies, the methods can be divided into two families [1–3]: the discontinuous and the continuous approaches. The rigid body assumption made here means that the bodies are supposed to be hard and only very small local deformations are required to generate very large contact pressures [4]. The discontinuous approaches assume that the impact occurs instantaneously and changes the momenta balances of the system instantaneously, see e.g. [5, 6]. In [7] the impact is considered also discontinuous, but a fast time scale, which considers the duration of the contact and the flexibility of the colliding bodies, is used to compute the coefficient of restitution to feed back the multibody system equations. On the other hand, the continuous approaches are based on regularized-force models that relate the force and deformation of the bodies in collision [1, 8], or based on unilateral constraints techniques that avoid the penetration between bodies [9–12]. In applications in which permanent contacts or at least contacts of a significant duration are expected to occur, continuous methods are needed. The continuous methods based on regularized forces include a number of viscoelastic and viscoplastic models (see e.g. [3, 13, 14, 25]).

Between the large number of existent formulations of the equations of motion (see e.g. [15]), the penalty and augmented Lagrangian formulations [17, 18] are characterized by transforming the constraints into forces proportional to the constraints violation. This technique, used along this work, is similar and compatible to that of the continuous-force models for normal contact, which relate the force and deformation of the bodies in contact to avoid the penetration between them.

It is worth to mention that, up to these days, no universally accepted model has been developed for the friction force between bodies under dry conditions. The Coulomb's friction law is the most simple model but has the problem that, when used along with continuous normal force models, the gradient of the force at null tangential velocity is infinite. This fact is unacceptable from the numerical point of view, since the motion has to be solved in discrete time-steps and it is not possible to deal with an infinite gradient at null velocity in these conditions (see e.g. [19]). The solution is to avoid the discontinuity of the Coulomb's model while maintaining the physical characteristics of the friction phenomenon important for the considered application [3]. For this paper a tangential friction model was developed to deal with the applications tackled; the model includes Coulomb's friction, sticktion at low velocities and a viscous friction term. Including the sticktion is indispensable for applications like the excavator simulator presented in this paper, since the excavator works on its legs and blade, for example, on slopes.

Related to the contact models, there are two difficult problems to address in real-time applications, especially when using constant integration time-step, which is the case here. The first one is the fact that the contact takes place in a limited, and sometimes very reduced, number of time steps, so that the algorithm has to be robust enough to overcome hard impacts; the second one was mentioned before and is related to the stability of the friction forces at low velocities and the transition between slipping and sticking.

This work explains the treatment chosen by the authors to address the contact between bodies in an excavator simulator for training personnel, which is an application subject to all the restrictions mentioned in the last paragraphs. The solution fulfills all the requirements proposed in terms of efficiency, robustness, and precision in the physical behavior.

2 Description of the multibody formalism

The multibody formulation chosen for this work is an index-3 augmented Lagrangian with projections of velocities and accelerations onto the constraints manifolds. The multibody modeling of the systems is done in natural coordinates [15, 16]. The formalism was extensively described in [20, 21]; for this reason, only a brief summary is given here.

The equations of motion are given by the following expressions:

$$\mathbf{M}\ddot{\mathbf{q}} + \mathbf{\Phi}_{\mathbf{q}}^{\mathrm{T}}\boldsymbol{\lambda}^{*} + \mathbf{\Phi}_{\mathbf{q}}^{\mathrm{T}}\alpha\mathbf{\Phi} = \mathbf{Q}(\mathbf{q}, \dot{\mathbf{q}}), \tag{1}$$

$$\boldsymbol{\lambda}_{i+1}^{*} = \boldsymbol{\lambda}_{i}^{*} + \alpha\mathbf{\Phi}_{i+1}, \quad i = 0, 1, 2, \ldots, \tag{2}$$

where $\mathbf{M}$ and $\mathbf{Q}$ are the mass matrix and generalized forces vector, $\mathbf{q}$ is the vector of natural coordinates of the system, $\mathbf{\Phi}$ and $\mathbf{\Phi}_{\mathbf{q}}$ are the constraints vector and its Jacobian matrix respectively and $\boldsymbol{\lambda}$ is the Lagrange multipliers vector. The scalar α is the penalty factor while the index i stands for the iteration number.

To integrate the equations of motion (1), the single-step trapezoidal rule is to be used. Since the mentioned integrator is implicit, establishing the dynamic equilibrium at time step $t + h$ (t being the simulation time and h the time step) leads to a nonlinear system of equations in the coordinates $\mathbf{q}$ for the time step. In order to obtain the solution of this nonlinear system, the Newton–Raphson method may be applied:

$$\left[\frac{\partial \mathbf{f}(\mathbf{q})}{\partial \mathbf{q}}\right]_{t+h}^{i} \Delta\mathbf{q}_{t+h}^{i+1} = -\left[\mathbf{f}(\mathbf{q})\right]_{t+h}^{i}, \tag{3}$$

$$\mathbf{q}_{t+h}^{i+1} = \mathbf{q}_{t+h}^{i} + \Delta\mathbf{q}_{t+h}^{i+1}, \tag{4}$$

where $\mathbf{f}(\mathbf{q})$ and $[\frac{\partial \mathbf{f}(\mathbf{q})}{\partial \mathbf{q}}]$ stand for the residual and tangent matrix of the nonlinear problem and have the following expressions:

$$\mathbf{f}(\mathbf{q}) = \frac{h^2}{4}\left(\mathbf{M}\ddot{\mathbf{q}} + \mathbf{\Phi}_{\mathbf{q}}^{\mathrm{T}}\lambda^{*} + \mathbf{\Phi}_{\mathbf{q}}^{\mathrm{T}}\alpha\mathbf{\Phi} - \mathbf{Q}\right), \tag{5}$$

$$\left[\frac{\partial \mathbf{f}(\mathbf{q})}{\partial \mathbf{q}}\right] \cong \mathbf{M} + \frac{h}{2}\mathbf{C} + \frac{h^2}{4}\left(\mathbf{\Phi}_{\mathbf{q}}^{\mathrm{T}}\alpha\mathbf{\Phi}_{\mathbf{q}} + \mathbf{K}\right). \tag{6}$$

In (6) the matrices $\mathbf{K}$ and $\mathbf{C}$ collect the contributions of the generalized forces vector derivatives to the tangent matrix, and can be considered as stiffness and damping matrices of the system:

$$\mathbf{K} = -\frac{\partial \mathbf{Q}}{\partial \mathbf{q}}, \tag{7}$$

$$\mathbf{C} = -\frac{\partial \mathbf{Q}}{\partial \dot{\mathbf{q}}}. \tag{8}$$

Once the convergence is achieved by (3) and (4), the velocities and accelerations obtained from the Newton–Raphson iteration, which will be called here $\dot{\mathbf{q}}^*_{t+h}$ and $\ddot{\mathbf{q}}^*_{t+h}$, are projected onto the constraints manifolds to obtain their cleaned counterparts, $\dot{\mathbf{q}}_{t+h}$ and $\ddot{\mathbf{q}}_{t+h}$, by means of the following expressions:

$$\left[\frac{\partial \mathbf{f}(\mathbf{q})}{\partial \mathbf{q}}\right]\dot{\mathbf{q}} = \left(\mathbf{M} + \frac{h}{2}\mathbf{C} + \frac{h^2}{4}\mathbf{K}\right)\dot{\mathbf{q}}^* - \frac{h^2}{4}\boldsymbol{\Phi}_{\mathbf{q}}^{\mathrm{T}}\alpha\boldsymbol{\Phi}_t, \tag{9}$$

$$\left[\frac{\partial \mathbf{f}(\mathbf{q})}{\partial \mathbf{q}}\right]\ddot{\mathbf{q}} = \left(\mathbf{M} + \frac{h}{2}\mathbf{C} + \frac{h^2}{4}\mathbf{K}\right)\ddot{\mathbf{q}}^* - \frac{h^2}{4}\boldsymbol{\Phi}_{\mathbf{q}}^{\mathrm{T}}\alpha\left(\dot{\boldsymbol{\Phi}}_{\mathbf{q}}\dot{\mathbf{q}} + \dot{\boldsymbol{\Phi}}_t\right), \tag{10}$$

$\boldsymbol{\Phi}_t$ being the partial derivatives of the constraints vector with respect to time.

3 Description of the contact model

The contact-forces approach proposed for this work comprises two different models: the normal-force model and the tangential-force model. The two models are presented separately in subsequent sections. The tangential model is an original contribution of this work while the normal model is completely taken from previous works.

As will be described later, in the human-in-the-loop application tackled in this paper the multibody model studied is divided into primitive objects (in the majority of the cases, spheres) for contact detection purposes, which interact with CAD environments composed of triangular meshes. Under these circumstances, all the contacts can be approximated as contacts between primitives and plane surface bodies. For simplicity, the case of spheres against plane surface bodies is the only case that will be explained here, but the generalization is straightforward.

3.1 Normal-force model

In order to choose the normal-force model, some tests were done with several continuous viscoelastic models, like the Hunt–Crossley model [8], the Lankarani–Nikravesh model [22], and the Kelvin–Voight model [23]. The results shown by the Hunt–Crossley and Lankarani–Nikravesh models where similar and very satisfactory while the Kelvin–Voight model suffered from a lack of dissipation in hard impacts, which must be solved in few time steps. Finally, the normal-force model chosen for this work was the Hunt–Crossley model [8]. The model is suited to collisions between massive solids for which the assumption of quasi-static contact holds and it can be supposed that the deformation is limited to a small region of the colliding bodies while the remainder of them are assumed to be rigid. The expression for the normal force, after some calculations, has the following form:

$$\mathbf{F}_n = k_n \delta^e \left(1 + \frac{3(1-\epsilon)}{2}\frac{\dot{\delta}}{\dot{\delta}_0}\right)\mathbf{n}, \tag{11}$$

where k_n is the equivalent stiffness of the contact which depends on the shape and material properties of the colliding bodies, e is the Hertz's exponent, $\delta = R_{\mathrm{sph}} - |\mathbf{p}_{\mathrm{center}} - \mathbf{p}_{\mathrm{contact}}|$ is the indentation, $\dot{\delta}$ its temporal derivative, $\dot{\delta}_0$ is the relative normal velocity between the colliding bodies when the contact is detected, ϵ is the coefficient of restitution, and $\mathbf{n}$ is the direction of the force (see Fig. 1). The subscript "n" comes from "*normal*."

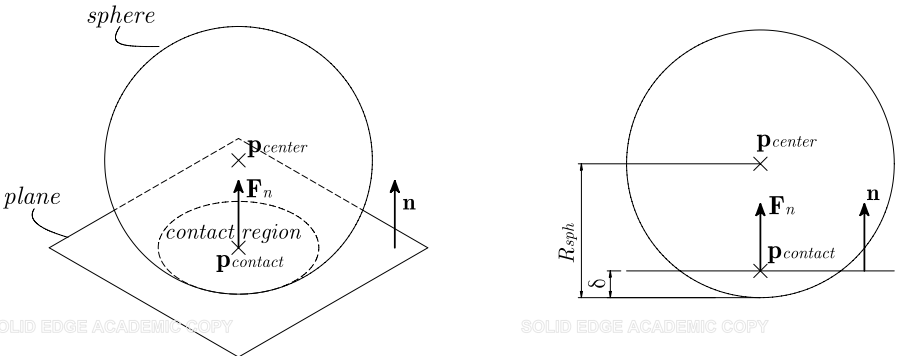

Fig. 1 Normal contact between sphere and plane: isometric and front views

The value of k_n can be calculated for general colliding paraboloids but, as was mentioned before, in this explanation all the contacts will be considered as contacts between spheres and plane surface bodies in which case the expression for the stiffness can be expressed by (see for example [24]):

$$k_n = \frac{4}{3(\sigma_{\text{sph}} + \sigma_{\text{pln}})}\sqrt{R_{\text{sph}}}, \tag{12}$$

where R_{sph} is the radius of the sphere in contact with the plane, and the material parameters of the sphere and plane, σ_{sph} and σ_{pln}, are given by

$$\sigma_{\text{sph}} = \frac{1-\nu_{\text{sph}}^2}{E_{\text{sph}}}, \qquad \sigma_{\text{pln}} = \frac{1-\nu_{\text{pln}}^2}{E_{\text{pln}}}, \tag{13}$$

with ν and E standing for the Poisson's ratio and the Young's modulus of each one of the two materials, represented by the sphere and plane.

It was explained in Sect. 2 that the formulation chosen for this work uses implicit integration and Newton–Raphson iteration and, therefore, the forces in the multibody system contribute to the tangent matrix (6) by means of the stiffness and damping matrices (7) and (8). For the Hunt–Crossley model presented here, the contribution to these matrices includes the following derivatives:

$$\mathbf{K}_n = -\frac{\partial \mathbf{F}_n}{\partial \mathbf{p}_{\text{center}}} = -\mathbf{n}\left(e\,k_n\delta^{e-1}\left(1+\frac{3(1-\epsilon)}{2}\frac{\dot{\delta}}{\dot{\delta}_0}\right)\right)\mathbf{n}^T, \tag{14}$$

$$\mathbf{C}_n = -\frac{\partial \mathbf{F}_n}{\partial \dot{\mathbf{p}}_{\text{center}}} = -\mathbf{n}\left(k_n\delta^e\left(\frac{3(1-\epsilon)}{2\dot{\delta}_0}\right)\right)\mathbf{n}^T. \tag{15}$$

These expressions are not yet the contributions to the tangent matrix of (6), because depending on the natural coordinates chosen in the construction of the multibody model, it is usually necessary to perform additional substitutions and derivatives to convert these expressions into derivatives of generalized forces with respect to generalized coordinates.

3.2 Tangential-force model

The tangential-force model developed for the friction force is based on Coulomb's law including sticktion. Moreover, a viscous term is added to the dry friction force. The general

form of this force is the following:

$$\mathbf{F}_t = \kappa \mathbf{F}_{\text{stick}} + (1-\kappa)\mathbf{F}_{\text{slide}} - \mu_{\text{visc}}\mathbf{v}_t. \tag{16}$$

In (16), the first two terms constitute the dry friction, while the third term accounts for the viscous friction. For the smooth transition between sticking and slipping, the dry friction force is divided into two components coupled by a smooth function, following the ideas proposed in [25]. The subscript "*t*" comes from "*tangential*."

In (16), μ_{visc} is the viscous damping coefficient, $\mathbf{F}_{\text{stick}}$ and $\mathbf{F}_{\text{slide}}$ are the components of the sticktion and slipping forces, κ is a smooth function of the tangential velocity, and $\mathbf{v}_t$ is defined in terms of the central point of the contact region, $\mathbf{p}_{\text{contact}}$, and the normal vector at the contact, $\mathbf{n}$, as follows:

$$\mathbf{v}_t = \dot{\mathbf{p}}_{\text{contact}} - \left(\mathbf{n}^{\text{T}}\dot{\mathbf{p}}_{\text{contact}}\right)\mathbf{n}. \tag{17}$$

The mentioned function, κ, has to match the following conditions:

$$\kappa = \left\{ \begin{array}{ll} 0; & |\mathbf{v}_t| \gg v_{\text{stick}} \\ 1; & |\mathbf{v}_t| = 0 \end{array} \right\}, \tag{18}$$

where v_{stick} is a parameter of the model accounting for the velocity of the stick–slip transition. A good choice for the transition function κ was given in [25] and has the following form:

$$\kappa = \mathrm{e}^{-(\mathbf{v}_t^{\text{T}}\mathbf{v}_t)/v_{\text{stick}}^2}. \tag{19}$$

Equation (16) showed that the total force is composed of three contributions: the sliding dry friction force at high velocities, the sticktion force at low velocities and the viscous friction force. The sticktion force will be considered by means of viscoelastic elements acting between the colliding bodies, called bristles. The expressions of the sliding and sticktion forces are given by (20) and (21) (see Fig. 2):

$$\mathbf{F}_{\text{slide}} = \left\{ \begin{array}{ll} 0; & |\mathbf{v}_t| = 0 \\ -\mu_{\text{din}}|\mathbf{F}_n|\frac{\mathbf{v}_t}{|\mathbf{v}_t|}; & |\mathbf{v}_t| > 0 \end{array} \right\}, \tag{20}$$

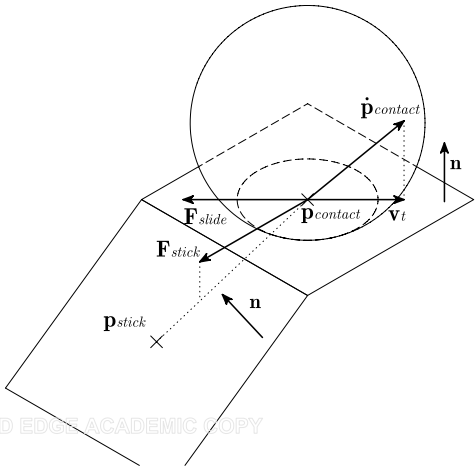

Fig. 2 Tangential contact between sphere and plane

$$\mathbf{F}_{\text{stick}} = \begin{cases} 0; & s = 0 \\ \frac{f^m_{\text{stick}}}{s}(\mathbf{I}_3 - \mathbf{n}\mathbf{n}^{\text{T}})(\mathbf{p}_{\text{contact}} - \mathbf{p}_{\text{stick}}); & s > 0 \end{cases}, \tag{21}$$

μ_{din} being the friction coefficient under dynamic conditions, $s = |\mathbf{p}_{\text{contact}} - \mathbf{p}_{\text{stick}}|$ the deformation of the bristles, with $\mathbf{p}_{\text{stick}}$ the sticktion point, which was initially the central point of the contact region in the instant at which the contact began; $\mathbf{I}_3$ is the identity matrix of size 3×3; f^m_{stick} is the function that represents the behavior of the bristles,

$$f^m_{\text{stick}} = -k_{\text{stick}}\, s - c_{\text{stick}}\, \dot{s}, \tag{22}$$

k_{stick} and c_{stick} being the stiffness and damping coefficients of the sticktion model. Nevertheless, there is a limiting value for the sticktion force:

$$|\mathbf{F}_{\text{stick}}| \leq \mu_{\text{st}} |\mathbf{F}_n|. \tag{23}$$

In (23), μ_{st} is the friction coefficient under static conditions which is, in general, higher than the dynamic friction coefficient. In case this limit is exceeded, and (23) is not fulfilled, there are two consequences: first, (22) is not valid anymore and (24) holds for the behavior of the bristles; second, the sticktion point has to be updated using (25)

$$f^m_{\text{stick}} = \frac{-\mu_{\text{st}} |\mathbf{F}_n| s}{|(\mathbf{I}_3 - \mathbf{n}\mathbf{n}^{\text{T}})(\mathbf{p}_{\text{contact}} - \mathbf{p}_{\text{stick}})|}, \tag{24}$$

$$\mathbf{p}_{\text{stick}} = \mathbf{p}_{\text{contact}} - \left(\frac{\eta_{\text{stick}} \mu_{\text{st}} |\mathbf{F}_n|}{k_{\text{stick}}} \right) \frac{\mathbf{v}_t}{|\mathbf{v}_t|}. \tag{25}$$

The coefficient η_{stick} controls the strain of the bristles when the maximum force is reached. Physically the more reasonable value is $\eta_{\text{stick}} = 1$, but small variations with $\eta_{\text{stick}} < 1$ can improve the numerical behavior of the model.

The contribution of the tangential force, $\mathbf{F}_t$, to the tangent matrix (6) includes the following derivatives.

1. Case $|\mathbf{F}_{\text{stick}}| \leq \mu_{\text{st}} |\mathbf{F}_n|$.

$$\mathbf{K}_t = -\frac{\partial \mathbf{F}_t}{\partial \mathbf{p}_{\text{contact}}} = \kappa \left(\mathbf{I}_3 - \mathbf{n}\mathbf{n}^{\text{T}}\right) \mathbf{K}^m_{\text{stick}} + (1 - \kappa) \mu_{\text{din}} \frac{\mathbf{v}_t}{|\mathbf{v}_t|} \frac{\partial |\mathbf{F}_n|}{\partial \mathbf{p}_{\text{contact}}}, \tag{26}$$

where

$$\mathbf{K}^m_{\text{stick}} = \frac{1}{s^2} \left(k_{\text{stick}} + \frac{f^m_{\text{stick}}}{s} \right) (\mathbf{p}_{\text{contact}} - \mathbf{p}_{\text{stick}}) (\mathbf{p}_{\text{contact}} - \mathbf{p}_{\text{stick}})^T - \frac{f^m_{\text{stick}}}{s} \mathbf{I}_3. \tag{27}$$

The damping contribution,

$$\begin{aligned} \mathbf{C}_t = -\frac{\partial \mathbf{F}_t}{\partial \dot{\mathbf{p}}_{\text{contact}}} &= \kappa \left(\mathbf{I}_3 - \mathbf{n}\mathbf{n}^{\text{T}}\right) \mathbf{C}^m_{\text{stick}} \\ &+ (1 - \kappa) \left[\mu_{\text{din}} \frac{\mathbf{v}_t}{|\mathbf{v}_t|} \frac{\partial |\mathbf{F}_n|}{\partial \dot{\mathbf{p}}_{\text{contact}}} + \frac{\mu_{\text{din}} |\mathbf{F}_n|}{|\mathbf{v}_t|} \left(\mathbf{I}_3 - \frac{\mathbf{v}_t \mathbf{v}_t^T}{|\mathbf{v}_t|^2} \right) \frac{\partial \mathbf{v}_t}{\partial \dot{\mathbf{p}}_{\text{contact}}} \right] \\ &+ \frac{2s}{v^2_{\text{stick}}} (\mathbf{F}_{\text{stick}} - \mathbf{F}_{\text{slide}}) \mathbf{v}_t^{\text{T}} \frac{\partial \mathbf{v}_t}{\partial \dot{\mathbf{p}}_{\text{contact}}} + \mu_{\text{visc}} \frac{\partial \mathbf{v}_t}{\partial \dot{\mathbf{p}}_{\text{contact}}}, \end{aligned} \tag{28}$$

being

$$\mathbf{C}^m_{\text{stick}} = \frac{c_{\text{stick}}}{s^2}(\mathbf{p}_{\text{contact}} - \mathbf{p}_{\text{stick}})(\mathbf{p}_{\text{contact}} - \mathbf{p}_{\text{stick}})^T, \tag{29}$$

$$\frac{\partial \mathbf{v}_t}{\partial \dot{\mathbf{p}}_{\text{contact}}} = \mathbf{I}_3 - \mathbf{n}\mathbf{n}^T. \tag{30}$$

2. Case $|\mathbf{F}_{\text{stick}}| > \mu_{\text{st}}|\mathbf{F}_n|$.

$$\mathbf{K}_t = \mathbf{0}, \tag{31}$$

$$\mathbf{C}_t = \mu_{\text{visc}} \frac{\partial \mathbf{v}_t}{\partial \dot{\mathbf{p}}_{\text{contact}}}. \tag{32}$$

It is important to note again that these expressions for $\mathbf{K}_t$ and $\mathbf{C}_t$ are not yet the contributions to the tangent matrix (6), because depending on the natural coordinates chosen in the construction of the multibody model, it is usually necessary to perform additional substitutions and derivatives to convert these expressions into derivatives of generalized forces with respect to generalized coordinates.

4 Contacts detection technique and computational aspects

The methods developed in this work are designed for applications in which contact plays an important role and, moreover, the multibody model or models have to interact with complex CAD environments. This is the case of simulators of certain kind of machinery and vehicles when the contact detection and all the calculations needed by the contact-force models have to be fast.

There are general contact detection techniques for multibody models whose geometry is given by complex CAD models [26], but sometimes the models are not fast enough to achieve real-time performance if a large number of bodies are considered or the geometries are too complex. For this reason, to deal with the kind of applications mentioned before, the technique used here is to approximate the environments and the multibody models by primitive objects: the complex CAD environments by meshes of triangular faces and the geometry of the multibody systems by spheres of different sizes (in the majority of the cases) and in some cases by boxes (when the geometry cannot be approximated by spheres in a satisfactory way). Each face of a CAD environment has its own normal vector and its own properties of stiffness and friction and each sphere is characterized also depending on the material properties and curvature of the multibody model.

The first step prior to the evaluation of the forces is to detect which faces of the environment collide with geometry of the multibody model. In Fig. 3 the different possibilities considered for contacts between primitive spheres and triangular faces are represented. The case of primitive boxes will not be considered here.

- The primitives are in contact when the distance, s, of the center of the sphere to the plane of the face is smaller than the radius of the sphere, R_{sph}, and the projection of its center on the plane lies inside the triangle (see Fig. 3(a)). In this case there is a contact between sphere and plane and the normal vector of the contact $\mathbf{n}$ is the normal vector of the plane of the face.

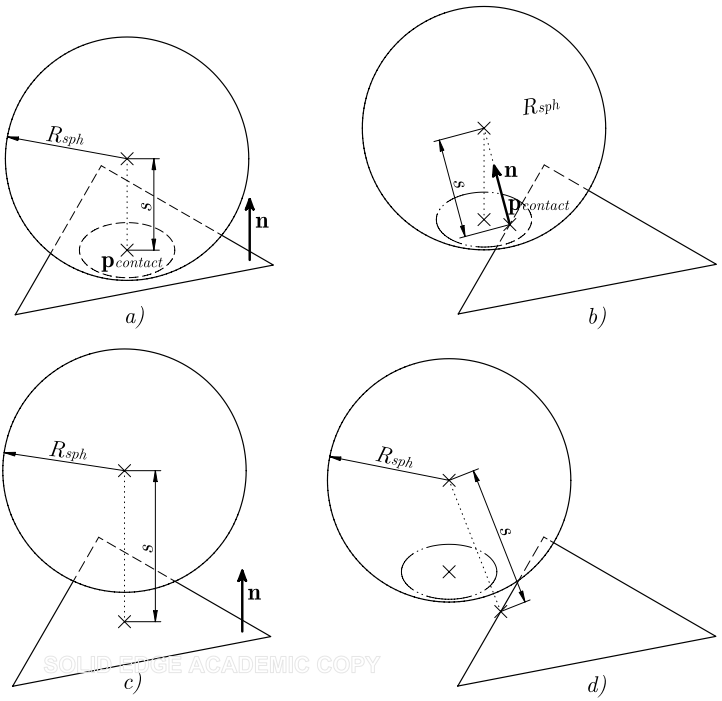

Fig. 3 Collision detection between sphere and triangular face

- When the previous conditions are not fulfilled, the primitives can be also in contact when the distance, s, of the center of the sphere to one of the edges of the face is smaller than the radius of the sphere, R_{sph}, and the projection of the center on the edge lies inside the edge (see Fig. 3(b)). In this case there is a contact between sphere and edge and the normal vector of the contact **n** has the direction from the contact point to the center of the sphere.
- If none of the previous situations happens, it is considered that the primitives are not in contact (see Fig. 3(c) and (d)). It is important to notice that the collisions between sphere and vertex are neglected here. This is an acceptable approximation which can lead to problems in environments with a lot of sharp points and non-convex geometry.

At each time step, the contact conditions have to be detected in a fast way. This involves checking all the spheres against all the faces and their edges, which means a lot of calculations per time step when the environments are realistic. In order to speed up this process, the algorithm uses an octree-based hierarchical decomposition of the entire scene mesh [27]. The bounds of the polygon soup are calculated through an Axis Aligned Bounding Box (AABB) to generate a tree-based hierarchical structure that is used to quickly reject the polygons not involved in potential collisions, in order to reduce the number of polygons tested against contact with the primitive objects that represent the geometry of the models. The depth of the tree has to be empirically optimized for speed.

Also, in order to save computational time, all the calculations necessary for computing the detections are reduced to the minimum. In this sense, many calculations would be precomputed like: all the equations of the planes of the meshes, certain constant expressions

used to decide if a point belonging to a plane is as well contained in the triangle of the face, the equations of the semi-infinite straight lines of the edges, and so on.

All the mentioned techniques not suffice for real-time purposes. As was described in Sect. 2, an implicit integrator is used with the aim of improving the stability of the integration and consequently the algorithm is iterative, which means that if all the calculations related to the contact detection were carried out in each iteration, the cost of the detection would rise in an uncontrollable manner as the number of iterations grow. The consequences of this would be completely unacceptable: as the integration becomes more difficult, the number of iterations grows and the computational cost of both the dynamics and the contact detection would grow as well. To avoid the testing of the whole tree of faces in each iteration, the faces susceptible to collision are selected after the prediction stage of the integrator and kept during the whole time step, i.e. once per time step instead of once per iteration, which helps to maintain the computational cost per time step more constant. Depending on the number of primitives present in the multibody model, the parallelization of the contact detection must be considered as well.

It is worth to mention that, in the strategy proposed in this work, the integration time-step is kept constant. On the one hand, this avoids difficult and cumbersome detections of the precise instant of contacts which makes the algorithm very simple, but, on the other hand, the strategy is very demanding for the integration algorithm since it has to overcome all the impacts and specially difficult situations present in the simulation without modifying the time step. Other works propose strategies for detection of the precise instant of contact (see [28]) and that would be the right approach to obtain accurate solutions when contacts occur but difficult to combine with the real-time requirements when a large number of contacts can take place at the same time.

5 Numerical examples

The formulation with the contact model proposed is tested in three different applications: the first one is the simulation of a spring–mass system with Coulomb's friction, which is an academic problem with known analytical solution; the second application is the well-known Bowden and Leben stick–slip experiment; the third application is the simulation of the whole model of a hydraulic excavator Liebherr A924, implemented as part of an excavator simulator, which is a realistic example that gives an idea of the capabilities of the method and the behavior of the simulations.

In all the examples of this work, the contact forces were included by means of the normal-force model explained in Sect. 3.1 and the tangential-force model developed in Sect. 3.2.

The mass–spring and Bowden and Leben stick–slip examples (Sects. 5.1 and 5.2) were implemented in Fortran 2003 language. The Liebherr A 924 excavator (Sect. 5.3) was implemented in Fortran 2003 language too, except for the graphics and collision detections, implemented in C++ language.

5.1 Mass–spring system with Coulomb's friction

The first system to be simulated is the mass–spring system with Coulomb's friction shown in Fig. 4, which is a very simple example with known analytical solution but at the same time interesting to test the tangential contact model proposed and to compare it with the known theoretical results.

The total time of simulation is 13 seconds and the time step h is 0.01 seconds. The system undergoes the influence of the gravity forces $g = 9.81\ \mathrm{m/s^2}$. The numerical values of the

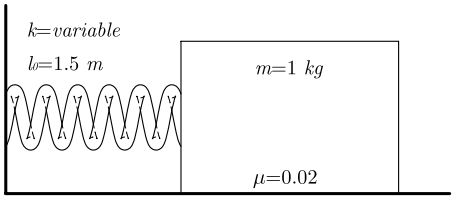

Fig. 4 Mass–spring system with Coulomb's friction

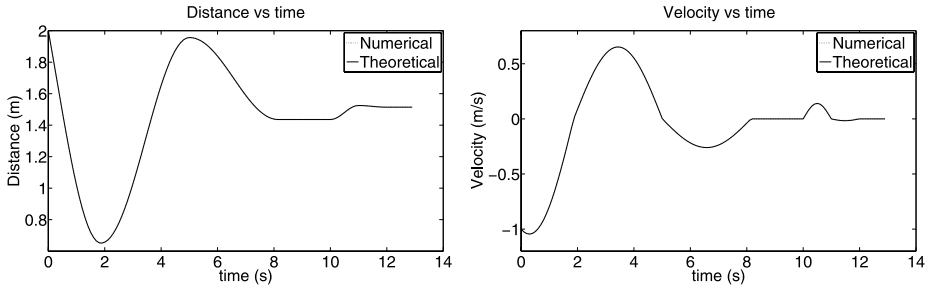

Fig. 5 Response of the system (block position and velocity): theoretical vs. numerical

parameters are: the mass of the block $m = 1$ kg, the dynamic friction coefficient $\mu_{\text{din}} = 0.02$, the static friction coefficient $\mu_{\text{st}} = \mu_{\text{din}}$, while the viscous friction coefficient $\mu_{\text{visc}} = 0$, the natural spring length $l_0 = 1.5$ m, the stiffness coefficient of the spring is $k = \left\{ \begin{smallmatrix} 1 \text{ N/m}; & t<10 \text{ s} \\ 10 \text{ N/m}; & t \geq 10 \text{ s} \end{smallmatrix} \right\}$, t being the integration time variable. The change on the spring stiffness is motivated to force the stick–slip transition when the simulation time reaches $t = 10$ s; just before this instant the mass was stuck to the plane and the change in the spring stiffness forced the mass to move.

For this example the actual geometry of the block is neglected and only two contact points are considered, one at each end of the block. The normal and tangential forces are introduced to these points. The block is constrained to move and rotate in the plane of the figure, so the system has 3 degrees of freedom.

The parameters of the normal-force model have little influence in the response (provided the stiffness of the contacts is sufficient and the restitution coefficient is not close to 1).

The remaining parameters for the tangential contact model described in Sect. 3.2 have the following values: $v_{\text{stick}} = N\mu gh$, $k_{\text{stick}} = m/(Nh)^2$, $c_{\text{stick}} = 2\sqrt{k_{\text{stick}} m}$, $\eta_{\text{stick}} = 1$. The parameter N allows to estimate the rest of parameters of the model and intends to be the number of time steps to stop the mass once the sticktion is acting, and is set to $N = 5$ for this application. Excessively low values lead to numerical problems.

The theoretical responses of the system vs. the numerical responses are shown in Fig. 5, the magnitudes represented are the block position (spring distance) and the block velocity (spring distance derivative). The coincidence between the theoretical and numerical responses is quite good, and the slip–stick and stick–slip transitions are also satisfactory.

5.2 The Bowden and Leben stick–slip experiment

The second system to be simulated is the Bowden and Leben stick–slip experiment. This experiment was first proposed by Bowden and Leben to study the stick–slip process [29] and it was described and solved recently in [25].

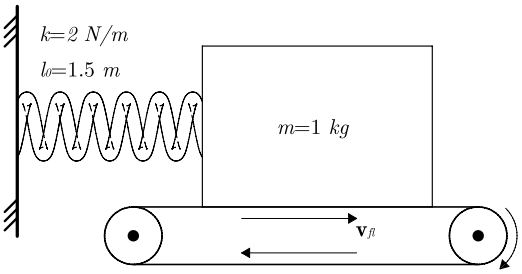

Fig. 6 The Bowden and Leben stick–slip experimental apparatus

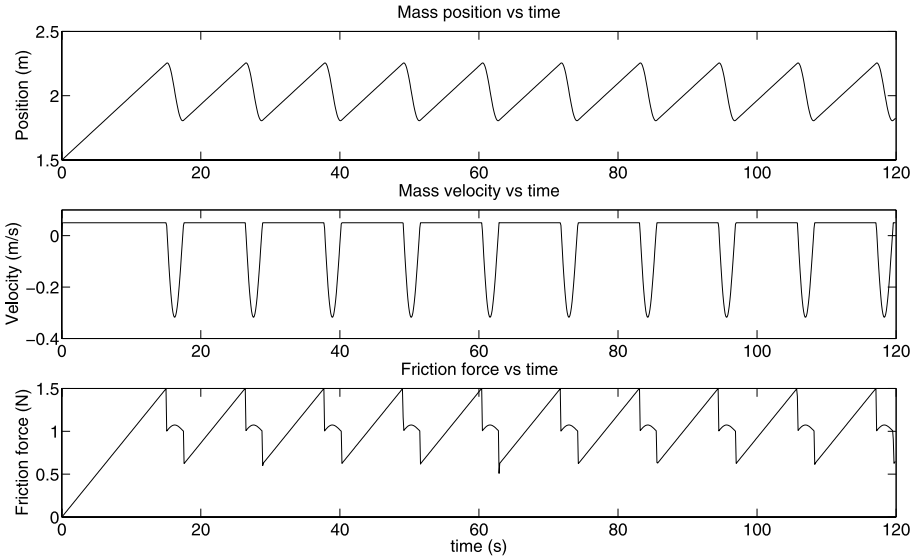

Fig. 7 Response of the system: (**a**) block position, (**b**) block velocity and (**c**) friction force

The system consists of a mass–spring system similar to that presented in Sect. 5.1 but, in this case, the block is mounted on a conveyor belt that is moved at a constant speed as shown in Fig. 6.

The simulation total time is 120 seconds and the time step h is 0.001 seconds. The system undergoes the influence of the gravity forces $g = 10$ m/s^2. The numerical values of the parameters are: the mass of the block $m = 1$ kg, the dynamic friction coefficient $\mu_{\text{din}} = 0.1$, the static friction coefficient $\mu_{\text{st}} = 0.15$, the viscous friction coefficient $\mu_{\text{visc}} = 0.1$, the natural spring length $l_0 = 1.5$ m, the stiffness coefficient of the spring is $k = 2$ N/m and the velocity of the conveyor belt is $\mathbf{v}_{fl} = 0.05$ m/s ("*fl*" for floor).

Like in the previous example, the actual geometry of the block is neglected and only two contact points are considered, one at each end of the block and the contact forces are introduced to these points.

The remaining parameters for the tangential contact model described in Sect. 3.2 have the following values: $v_{\text{stick}} = 0.001$ m/s, $k_{\text{stick}} = 10^5$ N/m, $c_{\text{stick}} = \sqrt{10^5}$ N s/m, $\eta_{\text{stick}} = 1$.

The responses of the system are shown in Fig. 7, the magnitudes represented are the block position (spring distance), the block velocity (spring distance derivative) and the magnitude of the friction force.

Note in Fig. 7(b) that the block is stuck to the conveyor belt until the spring force equals the maximum friction force available under static conditions ($\mu_{st}mg$). At this moment the block begins to slide and the maximum friction force available abruptly drops to the maximum force under dynamic conditions ($\mu_{din}mg$). Moreover, due to the relative velocity between the block and the conveyor belt, the viscous friction acts ($\mu_{visc}v_t$), which is responsible for the small round peaks that can be observed in Fig. 7(c). Finally, the block sticks again to the conveyor belt with a sticktion force that is much lower than the maximal available.

The response of the model presented here is very similar to that presented in [25], except that the model presented here does not take into account the dwell-time dependency of the sticktion force.

5.3 Liebherr A924 excavator

The modeled machine is a Liebherr A924 Litronic (see Fig. 8), a medium-size wheeled excavator. All the technical parameters of the real machine were taken from information provided by the manufacturer [31]. The time step chosen for the simulator is 5 milliseconds and the number of iterations of the implicit integrator is limited to 10 to guarantee the real-time performance, although this limit is rarely reached.

The machine has been modeled with 14 rigid bodies and 14 revolute joints, and is shown in Fig. 9. Elements crucial for stability like the front stabilizer blade and the left and right lateral outriggers (rear retractable legs) have been included in the model. Kinematics of the machine has been modeled with natural coordinates [15, 16], plus some distance and angular coordinates. The resulting excavator model has 154 coordinates (including 6 distances and 7 angles) and 154 constraints, 10 of them being redundant, which means that the excavator model has 10 degrees of freedom: 6 from the undercarriage free motion and 4 from the wheels rotation.

The external forces applied to the model are the following:

1. The weight of the machine parts and the bucket load.
2. The tire contact forces, which consist of linear spring and damper elements for the normal forces, and the magic formula tire model for the tangential forces [30].
3. Torques between undercarriage and wheels due to the accelerator and brake pedals action.
4. The contact forces originating from the collision of the excavator with the terrain or the surrounding objects; the contact model and the collisions detection technique were described in Sects. 3 and 4.

Fig. 8 Virtual excavator in its working environment

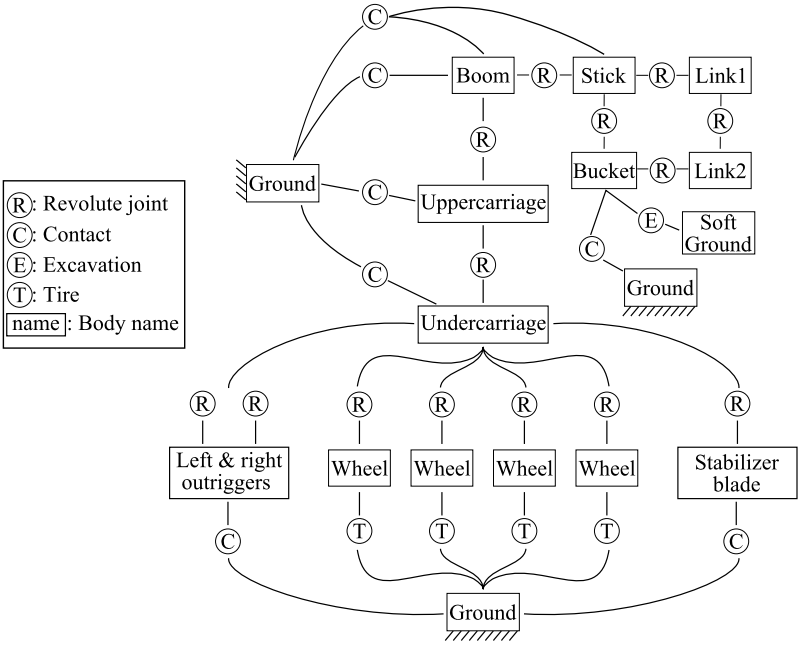

Fig. 9 Excavator's multibody model topology

Moreover, there are 6 actuators controlled by the operator. All the actuators have been modeled as rheonomic constraints acting on angular and distance variables, since the dynamics of the hydraulic circuit has not been considered in this version of the simulator.

1. Steering: the steering system actuates the front wheels and is modeled as a rheonomic constraint on an angular variable. Wheel's turns are related to the guided angular variable by the Ackerman's condition.
2. Uppercarriage rotary actuator: is modeled as a rheonomic constraint on an angular variable defined between the uppercarriage (cab) and the undercarriage (chassis).
3. Boom hydraulic cylinders: one rheonomic constraint on the cylinder distance variable models the two redundant hydraulic cylinders of the real machine.
4. Stick hydraulic cylinder: is modeled as one rheonomic constraint on the cylinder distance variable.
5. Stick hydraulic cylinder: is modeled as one rheonomic constraint on the cylinder distance variable.
6. Bucket hydraulic cylinder: is modeled as one rheonomic constraint on the cylinder distance variable.
7. Stabilizer blade and outriggers hydraulic actuators: in the real machine, three hydraulic cylinders control the simultaneous descent of the blade and outriggers. In the model, kinematic constraints relate the motion of the blades and outriggers, so that all of them can be controlled with an only rheonomic constraint on a distance variable.

Since the dynamics of the hydraulic circuit has not been modeled yet, the operator controls the position of the actuators without any delay or inertial effects. However, a simplified dynamics has been implemented for the actuators and the values of the Lagrange multipliers are verified to limit the force available according to the torques and lift capacities given

Fig. 10 Using the arm for descending a steep slope and terrain excavation

Fig. 11 Interacting with movable objects: breaking down fences and digging

by the manufacturer. Also, the velocities and accelerations of these kinematically guided actuators have been adjusted to match the technical specifications of the real machine.

The excavator is placed in a working environment (in Fig. 8 standing on its legs and blade), where the operator can perform different training exercises: maneuvering, digging, material handling, etc. The excavator interacts with the environment in two ways (see Fig. 10): (a) collisions with the scene objects and the terrain, which generate contact forces; and (b) terrain excavation and loading with the bucket.

Some scene objects are fixed (e.g. buildings, terrain) while others are movable (e.g. fences) as can be seen in Fig. 11. In order to compute the dynamics of movable objects, they are introduced in/removed from the simulation only when the excavator approaches/moves away from them; this technique makes possible to simulate in real-time working environments with a large number of movable objects.

The selected contact model delivers very realistic behavior and is able to simulate common events in the daily work of real excavators: slipping on slope terrains, stabilizing the machine with the blade and the outriggers (Fig. 8), using the arm for support or impulsion (Fig. 10), moving objects with the bucket or blade (Fig. 11), etc., or even other dangerous events not so common in the daily work, like rolling the excavator over (Fig. 12).

6 Conclusions

An integral solution to address contacts between solids in human-in-the-loop applications was described. The algorithm presented to integrate the equations of motion uses constant time-step and implicit integration, avoiding difficult and cumbersome detections of the precise instant of contact, modifications of the time step and re-starts of integration process.

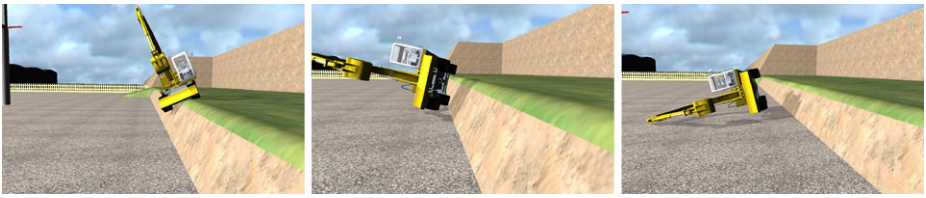

Fig. 12 Excavator rollover

The strategy of constant integration time-step is very demanding for the integration algorithm since it has to overcome all the impacts and specially difficult situations present in the simulation without modifying the time step. The strategy has many advantages because of its simplicity but the main drawback is that the precision of the solution is not constant along the simulation.

A new tangential contact force model was developed which includes sliding friction force, sticktion force and viscous friction force. The new model was successfully combined with some well-known normal contact force models. Between all the normal models tested, the Hunt–Crossley model [8] was chosen for the simulations carried out in this work as the model that better combines with the new model.

The contact detection technique was described and computational aspects were taken into account along this work, which are crucial to achieve real-time performance.

The contact-force model (combination of normal and tangential forces) was implemented in two academic examples, showing that it observes the physical laws of the phenomenon and the behavior of the algorithm is very good.

Finally, the proposed contact solution (including the contacts-detection technique, normal-force and tangential-force models and advanced computational aspects) was implemented in a real-time multibody model of a hydraulic excavator which is part of an excavator simulator, showing a wonderful behavior in the most common operation events of the daily work of this kind of machinery.

References

1. Lankarani, H.M., Nikravesh, P.E.: A contact force model with hysteresis damping for impact analysis of multibody systems. J. Mech. Des. **112**, 369–376 (1990)
2. Flores, P., Ambrosio, J., Claro, J.C.P., Lankarani, H.M.: Influence of the contact-impact force model on the dynamic response of multi-body systems. Proc. Inst. Mech. Eng., Proc. Part K, J. Multi-Body Dyn. **220**, 21–34 (2006)
3. Flores, P., Ambrosio, J., Claro, J.C.P., Lankarani, H.M.: Kinematics and Dynamics of Multibody Systems with Imperfect Joints. Springer, Berlin (2008)
4. Stronge, W.J.: Impact Mechanics. Cambridge University Press, Cambridge (2004)
5. Djerassi, S.: Collision with friction. Part A: Newton's hypothesis. Multibody Syst. Dyn. **21**, 37–54 (2009)
6. Djerassi, S.: Collision with friction. Part B: Poisson's and Stronge's hypotheses. Multibody Syst. Dyn. **21**, 55–70 (2009)
7. Schiehlen, W., Seifried, R.: Three approaches for elastodynamic contact in multibody systems. Multibody Syst. Dyn. **12**, 1–16 (2004)
8. Hunt, K.H., Crossley, F.R.E.: Coefficient of restitution interpreted as damping in vibroimpact. J. Appl. Mech. **7**, 440–445 (1975)
9. Lotstedt, P.: Mechanical systems of rigid bodies subject to unilateral constraints. SIAM J. Appl. Math. **42**, 281–296 (1982)
10. Pfeiffer, F., Glocker, C.: Multi-body Dynamics with Unilateral Constraints. Wiley, New York (1996)

11. Bhalerao, K.D., Anderson, K.S., Trinkle, J.C.: A recursive hybrid time-stepping scheme for intermittent contact in multi-rigid-body dynamics. J. Comput. Nonlinear Dyn. **4**, 281–296 (2009)
12. Flores, P., Leine, R., Glocker, C.: Modeling and analysis of planar rigid multibody systems with translational clearance joints based on the non-smooth dynamics approach. Multibody Syst. Dyn. **23**, 165–190 (2010)
13. Ismail, K.A., Stronge, W.J.: Impact of viscoplastic bodies: dissipation and restitution. J. Appl. Mech. **75**, 1–5 (2008)
14. Butcher, E.A., Segalman, D.J.: Characterizing damping and restitution in compliant impacts via modified K-V and higher-order linear viscoelastic models. J. Appl. Mech. **67**, 831–834 (2000)
15. Garcia de Jalon, J., Bayo, E.: Kinematic and Dynamic Simulation of Multibody Systems: The Real-time Challenge. Springer, Berlin (1994)
16. Garcia de Jalon, J.: Twenty-five years of natural coordinates. Multibody Syst. Dyn. **18**, 15–33 (2007)
17. Bayo, E., García de Jalon, J., Serna, M.A.: A modified lagrangian formulation for the dynamic analysis of constrained mechanical systems. Comput. Methods Appl. Mech. Eng. **71**, 183–195 (1988)
18. Bayo, E., Ledesma, R.: Augmented Lagrangian and mass-orthogonal projection methods for constrained multibody dynamics. Nonlinear Dyn. **9**, 113–130 (1996)
19. Eich-Soellner, E., Führer, C.: Numerical Methods in Multibody Dynamics. Teubner, Stuttgart (1998)
20. Cuadrado, J., Gutierrez, R., Naya, M.A., Morer, P.: A comparison in terms of accuracy and efficiency between a MBS dynamic formulation with stress analysis and a non-linear FEA code. Int. J. Numer. Methods Eng. **51**, 1033–1052 (2001)
21. Cuadrado, J., Dopico, D., Naya, M.A., Gonzalez, M.: Penalty, semi-recursive and hybrid methods for MBS real-time dynamics in the context of structural integrators. Multibody Syst. Dyn. **12**, 117–132 (2004)
22. Lankarani, H.M., Nikravesh, P.E.: Continuous contact force models for impact analysis in multibody systems. Nonlinear Dyn. **5**, 193–207 (1994)
23. Zukas, J.A., Nicholas, T., Greszczuk, L.B., Curran, D.R.: Impact Dynamics. Wiley, New York (1982)
24. Goldsmith, W.: Impact, the Theory and Physical Behaviour of Colliding Solids. Edward Arnold, London (1960)
25. Gonthier, Y., McPhee, J., Lange, C., Piedboeuf, J.C.: A regularized contact model with asymmetric damping and dwell-time dependent friction. Multibody Syst. Dyn. **11**, 209–233 (2004)
26. Choi, J., Ryu, H.S., Kim, C.W., Choi, J.H.: An efficient and robust contact algorithm for a compliant contact force model between bodies of complex geometry. Multibody Syst. Dyn. **23**, 99–120 (2010)
27. Foley, J.D., van Dam, A., Feiner, S.K., Hughes, J.: Introduction to Computer Graphics. Addison-Wesley, Reading (1993)
28. Flores, P., Ambrosio, J.: On the contact detection for contact-impact analysis in multibody systems. Multibody Syst. Dyn. **24**, 103–122 (2010)
29. Rabinowicz, E.: Stick and slip. Sci. Am. **194**(5), 109–118 (1956)
30. Pacejka, H.B., Bakker, E.: The magic formula tyre model. In: Pacejka, H.B. (ed.): Tyre Models for Vehicle Dynamics Analysis. Taylor & Francis, London (1993)
31. Liebherr-International Deutschland GmbH. Technical description A 924 C Litronic. http://www.liebherr.com/lh/en/ (2008)